

Vertical Velocity Variance in the Mixed Layer from Radar Wind Profilers

Ken Eng¹; Richard L. Coulter²; and Wilfried Brutsaert³

Abstract: Vertical velocity variance data were derived from remotely sensed mixed layer turbulence measurements at the Atmospheric Boundary Layer Experiments (ABLE) facility in Butler County, Kansas. These measurements and associated data were provided by a collection of instruments that included two 915 MHz wind profilers, two radio acoustic sounding systems, and two eddy correlation devices. The data from these devices were available through the Atmospheric Boundary Layer Experiment (ABLE) database operated by Argonne National Laboratory. A signal processing procedure outlined by Angevine et al. was adapted and further built upon to derive vertical velocity variance, $\overline{w'^2}$, from 915 MHz wind profiler measurements in the mixed layer. The proposed procedure consisted of the application of a height-dependent signal-to-noise ratio (SNR) filter, removal of outliers plus and minus two standard deviations about the mean on the spectral width squared, and removal of the effects of beam broadening and vertical shearing of horizontal winds. The scatter associated with $\overline{w'^2}$ was mainly affected by the choice of SNR filter cutoff values. Several different sets of cutoff values were considered, and the optimal one was selected which reduced the overall scatter on $\overline{w'^2}$ and yet retained a sufficient number of data points to average. A similarity relationship of $\overline{w'^2}$ versus height was established for the mixed layer on the basis of the available data. A strong link between the SNR and growth/decay phases of turbulence was identified. Thus, the mid to late afternoon hours, when strong surface heating occurred, were observed to produce the highest quality signals.

DOI: 10.1061/(ASCE)1084-0699(2003)8:6(301)

CE Database subject headings: Wind velocity; Radar; Variance analysis; Measurement; Wind; Turbulent boundary layers; Turbulence.

Introduction

Turbulence in the mixed layer has traditionally been measured by a variety of devices, most notably, tower platforms and aircraft. Few towers are available where needed and usually they are not tall enough to provide measurements throughout the mixed layer. Aircraft are expensive to operate; moreover, measurements by aircraft in the mixed layer are typically noisy and, especially near the top of the mixed layer or inversion base, difficult to obtain. In recent years a better alternative has become available by the advent of ground-based remote sensing equipment. This type of equipment is nonintrusive to the flow, requires little maintenance, and is capable of measuring continuously throughout the year. Measurements from two radar-type 915 MHz wind profilers/radio acoustic sounding systems (915 MHz WP/RASS) were chosen to provide the data on turbulence in the mixed layer for this study. An inherent weakness of ground-based remote sensing equipment is the quality of the return signal, represented by the signal-to-

noise ratio, SNR. Angevine et al. (1994a), for example, applied quality control procedures on return signals from 915 MHz WP/RASS.

This paper aims to build upon the procedures outlined by Angevine et al. (1994a) for the return signals and to take them a step further for the present purpose. An analysis is presented of wind profile measurements obtained with 915 MHz WP/RASS to determine vertical velocity variance, $\overline{w'^2}$, in the mixed layer. In the process, a similarity relationship is established for the scaled vertical velocity within the mixed layer; this should have broader applicability than previous estimates, based on more limited data. In addition, the RASS is used to provide mixed layer heights and mixed layer virtual potential temperatures, which are used in the scaling.

Study Area and Instrumentation

The data used in this study were collected in 1997–1999 at the Atmospheric Boundary Layer Experiments (ABLE) facility (Wesely et al. 1997; Coulter et al. 1999). ABLE covered a major portion of the Walnut River watershed, located in Butler County, Kansas. The ABLE site is flat in the western portions and becomes gradually more hilly towards its eastern border. The land use is predominately a mix of cropland and grassland (Lemone et al. 2000).

The variables of interest in this study include the vertical velocity variance, $\overline{w'^2}$; the virtual potential temperature, θ_v ; the mixed layer height, z_i ; and the specific surface sensible heat flux, $w'\theta'_{vo}$ ($=H/\rho c_p$, where H =surface virtual sensible heat flux; ρ =density of the air; and c_p =specific heat at constant pressure). The $\overline{w'^2}$ values were obtained from two 915 MHz WP. These

¹Research Hydrologist, National Research Program, U.S. Geological Survey, 12201 Sunrise Valley Dr., Mail Stop 430, Reston, VA 20192.

²Meteorologist, Argonne National Laboratory, 9700 South Cass Ave., Argonne, IL 60439.

³Professor, School of Civil and Environmental Engineering, 220 Hollister Hall, Cornell Univ., Ithaca, NY 14853.

Note. Discussion open until April 1, 2004. Separate discussions must be submitted for individual papers. To extend the closing date by one month, a written request must be filed with the ASCE Managing Editor. The manuscript for this paper was submitted for review and possible publication on June 24, 2002; approved on February 7, 2003. This paper is part of the *Journal of Hydrologic Engineering*, Vol. 8, No. 6, November 1, 2003. ©ASCE, ISSN 1084-0699/2003/6-301–307/\$18.00.

Table 1. Relevant Instruments in ABLE

Location	Equipment	Measurement	Latitude and longitude
Beaumont, Kan.	One 915 MHz WP One RASS	$\overline{w'^2}$ (200 m to 2 km) θ_{ML} and z_i	37 37' 38" and 96 32' 19"
Smileyburg, Kan.	One sonic anemometer	H	37 31' 15" and 96 51' 18"
Whitewater, Kan.	One 915 MHz WP One RASS	$\overline{w'^2}$ (200 m to 2 km) θ_{ML} and z_i	37 51' 01" and 97 11' 15"
Towanda, Kan.	One sonic anemometer	H	37 50' 31" and 97 01' 12"

devices operate by transmitting electromagnetic energy into the atmosphere in five different directions: vertical and nonvertical beams to the north, south, east, and west offset from the vertical by approximately 14°. The 915 MHz WP measure the strength and frequency of the backscattered energy of the transmitted electromagnetic energy. These wind profilers scanned for roughly 30 s in each of the five directions in sequence. This operation took approximately 2.5 min to complete, after which the cycle was repeated. The $w'\theta'_{vo}$ values were furnished by two eddy correlation devices. The eddy correlation devices were three-dimensional sonic anemometers that measure wind components and temperature to estimate surface fluxes. The θ_v and z_i values were obtained from the radio acoustic sounding system (RASS) data. RASS measured in conjunction with the 915 MHz WP and used a similar operation but sent out sound waves in addition to the electromagnetic energy of the WP. The index of refraction changes by the acoustic wave front were used as the signal source. A list of all equipment used in this study, their location, and the measurements provided is given in Table 1. Since the eddy correlation devices were not at the same location as the 915 MHz WP and RASS instruments, it was assumed that solar radiation was roughly uniform over the study area. On very clear days, vegetation and soil moisture conditions can be assumed to be uniform over similar terrain, making this a reasonable assumption.

Signal Processing of Radar Wind Profilers

Two Different Scales of Variance

Turbulent motions in the atmosphere range in size from synoptic scales to scales where the viscosity dissipates these motions off as heat. Wind profiler data are affected by motions both larger and smaller than the scanned volume. The large scale variance, $\overline{w_L'^2}$, consists of motions larger than the resolution volume and is given by the time variation of the mean Doppler velocity measurements of the 915 MHz WP. The small scale variance, $\overline{w_s'^2}$, is made up of motions smaller than the resolution volume and contributes to the spectral width of the peak in the assembled spectra of the 915 MHz WP (Doviak and Zrnić 1993). To obtain the total variance, the small and the large scale variances are simply added together.

Determination of Vertical Velocity Variance

Before any signal processing procedures outlined in this study were applied, the raw data were subjected to two filters designed to remove outliers. The first filter simply compared outliers to adjacent values in time. The second filter screened out outliers by comparing each value within a subgroup of values to its mean and variance, and this methodology was repeated throughout all the data with other subgroupings. Coulter and Lesht (1997) and Ja-

cobs et al. (2000) have obtained reasonably good results utilizing this type of data. The vertically pointing beam measures $\overline{w'^2}$ values directly. Because the vertical components of the other four beams were available, they were averaged with the independent vertical beam to provide a more stabilized value of $\overline{w'^2}$ for $\overline{w_L'^2}$. The small and large scale vertical velocity variances were calculated for all the dates listed in Table 2 for 1200 CST (Central Standard Time), 1300 CST, 1400 CST, and 1500 CST (selection of these times and dates will be further discussed later in this paper) with the procedure outlined in the following two sections.

Small Scale Vertical Velocity Variance

The spectral widths, SW , are provided by the manufacturer as values in frequency space that are the fraction of the Nyquist frequency, f_N , which is, in turn, defined by operational parameters of the profiler. This is then converted to velocity space (Doviak and Zrnić 1993) as

$$V_{swv} = \frac{cf_N}{2f} SW \quad (1)$$

where V_{swv} = spectral width velocity in m/s; c = speed of light ($= 3 \times 10^8$ m/s); and f = frequency ($= 915$ MHz). Before the spectral width velocities were squared and averaged, they were subjected to a procedure outlined in Angevine et al. (1994a) that removed incorrect estimates of the wind and acoustic velocities by using statistical limits. This procedure was adjusted as follows.

One modification was to impose a SNR filter such that the return signal needed to be greater than or equal to a certain SNR cutoff value. The SNR for the wind profilers is given by

$$SNR = 10 \log_{10} \left(\frac{\text{Signal Power}}{\text{Noise Power}} \right) \quad (2)$$

which is expressed in decibels (dB). Each spectral width measurement had associated with it a SNR value to indicate the relative amount of noise in the return signal. Poor quality return signals were associated with low SNR values and good quality ones with high values. Return signals from the upper portions of the mixed layer inherently have a lower SNR associated with them due to geometrical divergence of the scattered signal. Therefore, a variable height SNR filter was used. For the first five measurement levels (145, 202, 260, 318, and 376 m), a more restrictive SNR filter was used while a less stringent one was used for the upper

Table 2. Dates Used in Study

Year	Month/Date
1997	5/9, 5/10, 5/11, 5/12, 5/16, 5/17, 5/20, 7/2, 7/31
1998	9/4
1999	6/2, 6/14, 7/21, 7/22, 7/25, 8/11, 8/12, 8/14, 8/15, 8/17, 8/18, 8/19

Table 3. SNR Filter Cutoff Values

Procedure	SNR (dB):	
	Lower height range	Upper height range
1	No filter	No filter
2	-1	-4
3	+3	0
4	+7	+4

five measurement levels (434, 491, 549, 607, and 665 m). The first measurement level of 87 m was ignored, because it is typically contaminated with ground clutter and electromagnetic interference. The point in the mixed layer where the SNR filter was changed was arbitrary, so this point was chosen roughly in the middle of the averaged mixed layer heights. Angevine et al. (1994a) suggested SNR limits of two standard deviations around the mean (i.e., mean $\pm 2\sigma$). Since it was not clear what value of SNR would denote a good versus a poor quality return signal, several cutoff values were tried. Table 3 lists all the SNR cutoff values tried in this study. As will be further discussed in a later section, procedure 3 generated the smallest amount of scatter yet retained a considerable amount of data and was therefore selected. Accordingly, the analyses presented in the remainder of this paper (except in the section titled "Sensitivity to SNR Filter Cutoff Values") will be based on procedure 3 values.

In the original procedure by Angevine et al. (1994a), removal of outliers was carried out on the spectral width velocity data outside of 2σ from the mean. In the present study, this removal was implemented instead on the squared values of the deviations. Besides natural noise, this removal also ensured removal of exceedingly large SNR values associated with planes and birds. In addition to these effects, similar systems to the ones used in the present study possess inherent biases due to other factors. Portions of this system bias were accounted for by the beam broadening effects and vertical shear of horizontal winds outlined in a study by Nastrom (1997). Nastrom (1997) proposed that the small scale vertical velocity variance values were equivalent to the observed vertical velocity variance minus the variance introduced by these two effects. By accounting for these two effects, the equations by Nastrom (1997) greatly reduced this bias in most cases, but rarely to zero. Angevine et al. (1994a) assumed that the mean small scale variance becomes negligible at the top of the mixed layer, and that the height minus one standard deviation represents the remaining system bias, also known as the "floor." The rationale for this assumption was that the mean small scale variance is minimal near the top of the boundary layer because the local surface sensible heat flux decreases to zero near this region. The floor was attributed to signal processing (window effects), meteorological mechanisms, and other unexplained factors (Angevine et al. 1994a). Consequently, the floor was taken to be the mean $\overline{w_s'^2}$ at the top of the mixed layer minus one standard deviation. In other words, the floor was taken in the manner of Angevine et al. (1994a), but after the additional elimination of the effects of beam broadening and vertical shear from the observed vertical velocity variance; it is felt that by accounting explicitly for these two effects on $\overline{w_s'^2}$, uncertainty of this floor value was practically eliminated. Moreover, individual floor values were calculated in the present analysis for each hour for all dates considered instead of a seven day average value as in earlier studies.

Large Scale Vertical Velocity Variance

The large scale vertical velocity variance, $\overline{w_L'^2}$, was found by squaring the fluctuation component of the mean Doppler velocity

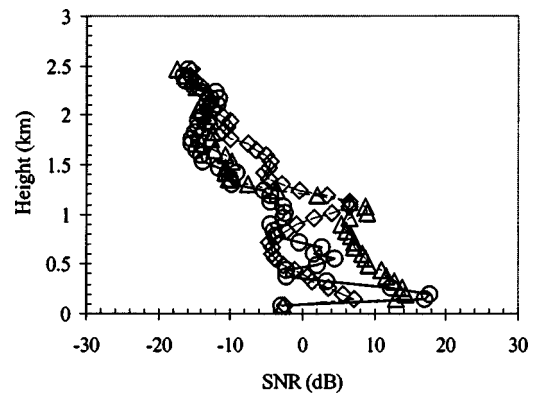


Fig. 1. Signal to noise ratio development throughout a day for the 915 MHz wind profiler/radio acoustic sounding system (WP/RASS) at Beaumont, Kan. on September 27, 1997. Signal to noise taken at 949–1049 CST (circles), 1349–1449 CST (triangles), and 1749–1849 CST (diamonds). The sharp increase is associated with the rapid rise of the rising mixed layer.

and then ensembled. The mean Doppler velocity, V_{md} , is calculated similar to the spectral width

$$V_{md} = \frac{cf_N}{2f} MDV \quad (3)$$

where V_{md} is in m/s; and MDV = mean Doppler value. The symbols c , f_N , and f are the same as in the previous section for $\overline{w_s'^2}$. In a similar way to $\overline{w_s'^2}$, the $\overline{w_L'^2}$ values were subjected to the SNR filter (procedure 3) mentioned in the previous section. Outliers were removed if the mean Doppler velocities fell out of the range of the mean $\pm 2\sigma$.

SNR–Height Time Evolution Link with Atmospheric Conditions

The optimal period for the best return signals of the 915 MHz WP was determined by analysis of the SNR evolution throughout a day. This analysis involved an examination of the hourly changes of the SNR versus height and atmospheric conditions for several cloudless days. In addition, the records with storm activity from six hours before to six hours after the times and dates were eliminated. This was done to prevent disturbances in the atmosphere from affecting the diurnal evolution of the boundary layer.

On clear and sunny days, the SNR versus height time evolution was linked to the growth/decay of the mixed layer or turbulence generation/breakdown, as illustrated in Fig. 1. The spike of high quality return signals in this figure has been associated with the rapid rise of the top of the mixed layer (Coulter 1979; Angevine et al. 1994b). Therefore, the times of a day when the 915 MHz WP generated the largest region of the best quality return signals were the early to mid afternoon hours (roughly 1200 CST to 1500 CST), when the mixed layer reached its largest depth. The dates used in this study are listed in Table 2.

Scaling Procedure

Mixed Layer Height and Average Virtual Potential Temperature

As will become clear hereafter, in order to scale the velocity variance it was necessary to determine the mixed layer height, z_i ,

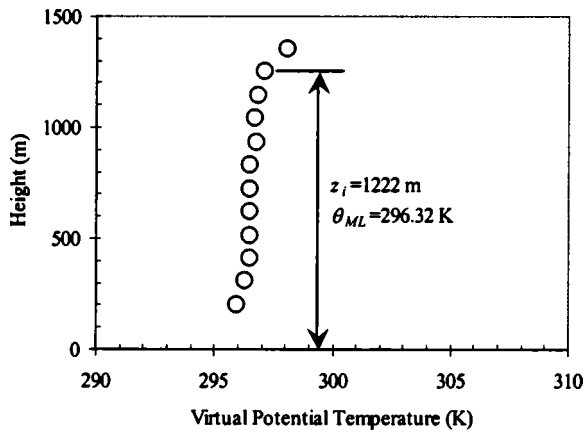


Fig. 2. Mixed layer height and virtual potential temperature determination from the radio acoustic sounding system (RASS) at Beaumont, Kan. at 1300 CST on June 14, 1999. Indicated heights are above ground surface.

and the virtual potential temperature, θ_v . In this study, RASS measurements were used for this purpose. The sounding system operated in RASS mode at the beginning of every hour. Therefore, 10 min averaged temperatures were taken before and after every hour considered and then averaged to produce one estimate. These 20 min estimates from RASS were then corrected for vertical wind velocities (e.g., Angevine et al. 1993) by

$$T_c = \frac{M_d(v-w)^2}{1.4R^*} - 273.15 \quad (4)$$

where T_c = virtual temperature in degrees Celsius; v = acoustic velocity in m/s; w = vertical wind velocity in m/s; M_d = molecular weight for dry air (= 28.96 grams/mole); R^*

= universal gas constant (= 8.314 kg m²/s² mole K); and 1.4 = ratio of specific heats for dry air (c_p/c_v). This corrected temperature, T_c , was then converted to virtual potential temperature by the approximate relationship

$$\theta_v = (T_c + 273.15) + (\Gamma_d z) \quad (5)$$

where Γ_d = dry adiabatic lapse rate (= 9.8 K/km); and z = elevation in kilometers. The RASS virtual potential temperatures were then plotted against height, and the region of nearly constant temperature was identified. The height of the top of this region was taken to be z_i and the bottom was often taken at the second measurement height of 203 m. The virtual potential temperatures in this zone were averaged to obtain the average mixed layer virtual potential temperature, θ_{ML} . An example of this outlined procedure is given in Fig. 2. Lower measurements below 100 m can be considered unreliable by these types of instruments due to ground clutter, so they were not included in the analysis. The z_i and θ_{ML} values for all the dates considered in this study are listed in Table 4. An example comparison of the RASS virtual potential temperatures with those obtained from the radiosonde profiles is shown in Fig. 3. This figure illustrates that the RASS instrument provides estimates of z_i and θ_{ML} , which are comparable to the values derived from radiosonde measurements.

Convective Vertical Velocity

The second moments of the turbulence in the mixed layer are usually scaled with the convective velocity scale, w_* ; this non-dimensionalization has the advantage that it should allow more universal application for any site and also comparison with previous experiments. This velocity scale is given by

$$w_* = \left[\frac{gz_i}{\theta_{ML}} (\overline{w'\theta'_{vo}}) \right]^{1/3} \quad (6)$$

Table 4. Values of Height of Mixed Layer, z_i , and Average Virtual Potential Temperature in Mixed Layer, θ_{ML}

Date (month/day/year)	1200 CST		1300 CST		1400 CST		1500 CST	
	z_i (m)	θ_{ML} (K)						
5/9/97	722	288.39	822	289.54	822	290.43	822	291.27
5/10/97	1,122	291.82	1,122	292.35	1,122	293.18	1,122	293.7
5/11/97	1,022	291.67	1,022	292.70	1,122	293.60	1,122	293.48
5/12/97	922	287.56	922	286.79	922	289.59	922	290.91
5/16/97	622	295.41	622	296.61	822	298.22	972	298.96
5/17/97	522	301.42	522	302.68	622	303.38	922	304.65
5/20/97	972	291.37	972	291.93	972	292.92	972	293.38
7/2/97	522	300.98	622	301.79	622	302.23	622	302.68
7/31/97	722	298.56	872	297.32	1,022	300.39	1,222	300.40
9/4/98	522	303.32	722	305.72	922	307.89	1,022	308.40
6/2/99	522	298.00	622	299.29	1,122	300.60	1,122	300.83
6/14/99	1,122	296.32	1,122	295.38	1,222	297.17	1,222	297.72
7/21/99	822	302.83	922	305.70	1,122	306.10	1,122	306.53
7/22/99	822	305.09	922	306.64	1,122	307.09	1,122	306.19
7/25/99	722	308.04	1,022	308.63	1,222	307.71	1,222	308.29
8/11/99	422	305.95	422	306.00	522	308.29	622	306.95
8/12/99	622	305.50	722	305.71	922	306.00	1,122	309.82
8/14/99	522	294.54	722	297.26	722	300.52	822	299.61
8/15/99	322	297.37	422	305.86	822	304.34	822	305.09
8/17/99	522	305.95	722	306.00	1,222	308.29	1,222	306.95
8/18/99	1,022	305.30	1,022	306.00	1,022	305.49	1,122	306.16
8/19/99	872	296.52	1,122	298.00	1,122	299.88	1,222	300.70

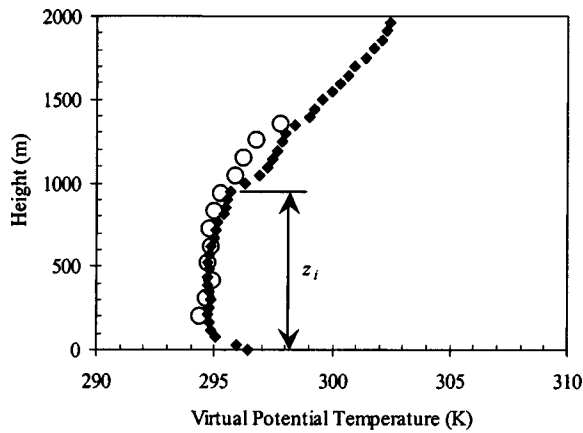


Fig. 3. Comparison between θ_v determined with a radiosonde (diamonds) and a radio acoustic sounding system (circles) for Whitewater, Kan. at 1400 CST on May 21, 1997. Indicated heights are above ground surface.

where g = acceleration of gravity; and $\overline{w'\theta'_{vo}}$ = specific flux of sensible heat at the surface. The variable w_* is a measure of the buoyancy effects in the atmosphere, and when it is scaled with friction velocity, $u_* (= [\tau_o/\rho]^{1/2})$, it plays the same role as the densimetric Froude number, the Richardson number, or z_i/L . Values of w_* were calculated with the z_i and θ_{ML} values listed in Table 4, and the $\overline{w'\theta'_{vo}}$ values were measured with the sonic anemometers.

Scaled Vertical Velocity Variance

The $\overline{w_s'^2}$ and $\overline{w_L'^2}$ values were added with a procedure 3 SNR filter described previously in the paper to obtain the total vertical velocity variance, $\overline{w'^2}$, for the times specified in Table 2. These $\overline{w'^2}$ values were then scaled with w_*^2 and plotted against scaled height, z/z_i , resulting in Fig. 4. A best fit curve is given by

$$\frac{\overline{w'^2}}{w_*^2} = A \left(\frac{z}{z_i} \right)^{2/3} \left[1 + C \left(\frac{z}{z_i} \right)^D \right] \quad (7)$$

where $A = 1.8$; $C = -0.934$; and $D = 0.720$.

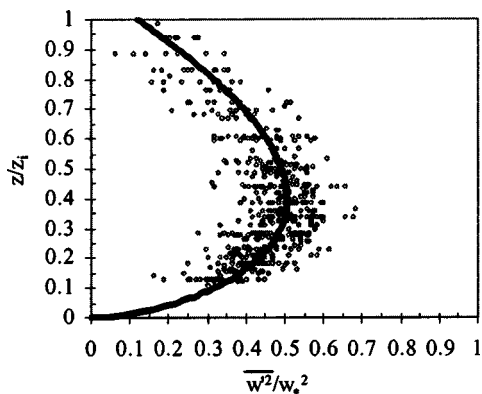


Fig. 4. Scaled vertical velocity variance values versus scaled height as processed with procedure 3 SNR filter limits (+3 dB for the lower and 0 dB for the upper levels). The solid curve is the best fit line and the circles represent each individual measurement.

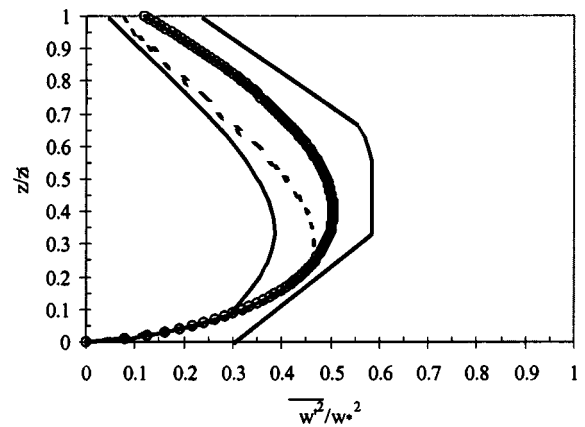


Fig. 5. Comparison between present result as given by Eq. (7) (solid line with circles) and results obtained in previous studies. Dashed line represents the empirical equation of Lenschow et al. (1980) and two solid lines represent the bounds set by Stull (1988) on the data obtained by Deardorff (1974), André et al. (1978), Thery and Lacarrère (1983), and Smedman and Högröm (1983).

General Features

In Fig. 5, it can be seen that $\overline{w'^2}/w_*^2$ values generated in this study compare well for the lower portions of the mixed layer with the empirical curve obtained by Lenschow et al. (1980) with aircraft measurements; they also fall well within the bounds of Stull's (1988) collection of data from other authors. At the base of the inversion layer, entrainment may be affecting the dimensionless vertical velocity variance; however, this will require further study. The scaled $\overline{w'^2}$ values were found to be close to normally distributed at each height level. As an example, the histogram and probability plot of these values at the $0.4 z/z_i$ height are presented as Figs. 6 and 7, respectively. Fig. 7 illustrates that nearly all of the scaled $\overline{w'^2}$ values fell within the 95% confidence intervals, suggesting that these values were normally distributed.

Sensitivity to SNR Filter Cutoff Values

The effect of the procedures listed in Table 3 on the scaled vertical velocity variance was examined. The results obtained with

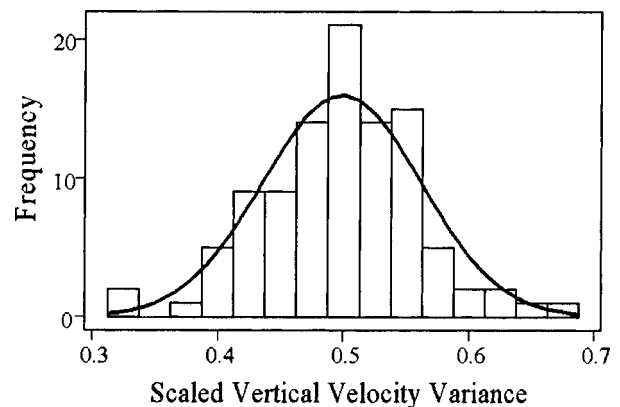


Fig. 6. Histogram plot of scaled vertical velocity variance values at the height $0.4 z/z_i$ for SNR filter cutoff values of +3 dB for the lower and 0 dB for the upper levels (procedure 3). The curve represents a normal distribution with the same mean and standard deviation as the histogram.

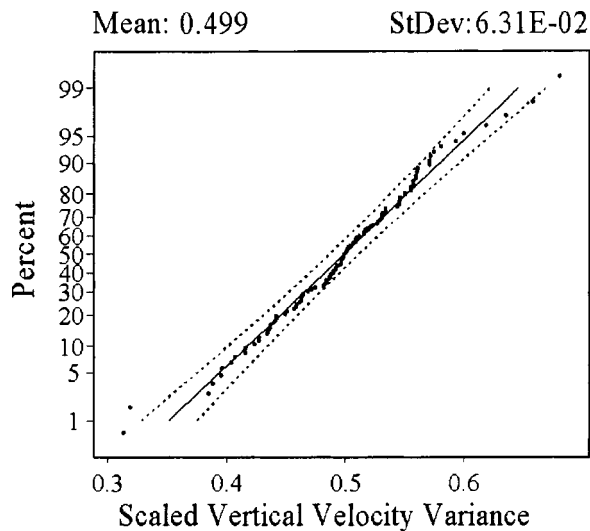


Fig. 7. Probability (of nonexceedance) of scaled vertical velocity variance values at the height of $0.4 z/z_i$ obtained with SNR filter cutoff values of +3 dB for the lower and 0 dB for the upper levels (procedure 3). The solid straight line represents the normal distribution with the same mean and standard deviation as the data; the dashed lines are the 95% confidence intervals.

SNR cutoff values of +3 dB for the lower and 0 dB for the upper levels (procedure 3) were presented in Fig. 4. Without removal of any signals (procedure 1), the mean scaled vertical velocity variance was lower while the standard deviation was larger than those shown in Fig. 4. This reduction in the mean value suggested that many of the small values of the scaled vertical velocity variance were associated with noise. Also, it stands to reason that, without any quality control on the return signals to the radar wind profilers, the introduction of signals with high SNR associated with planes, birds, and signals with low SNR linked to such effects as ground clutter will increase the standard deviation. A slightly more selective procedure of -1 dB for the lower and -4 dB for the upper levels was observed to produce a mean scaled vertical velocity variance that increased and a standard deviation that decreased from those in procedure 1, but still not to the levels shown in Fig. 4. The reduction of the standard deviation occurred due mainly to the removal of signals with very high and very low SNR. The mean value increased because the SNR filter had removed the signals with low SNR, which suggested again that some of the signals with low SNR were still linked more to noise and less to small scale vertical velocity variance values. The most restrictive procedure 4 with SNR filter cutoff values of +7 dB for the lower and +4 dB for the upper levels eliminated many of the dates considered in this study, and as a result the number of data points averaged at each level of z/z_i was reduced substantially. With these more restrictive limits, there was little improvement in the reduction of the standard deviation and little change in the mean value. Thus, the cutoff criterion used herein produced average values close to the asymptote obtained with more strict criteria; moreover, it yielded the smallest amount of spread about the mean while retaining a sufficient number of data points.

The effect of the SNR filter cutoff values on the distribution of the data at each height was investigated next. These plots for procedure 3 at $0.4 z/z_i$ were presented in Figs. 6 and 7. The raw data (procedure 1) produced scaled $\overline{w'^2}$ values that were generated by the physical turbulence and those which were associated with the system noise. Without SNR filter cutoff values, the

scaled $\overline{w'^2}$ values appeared to be normally distributed, because the majority of the data values were found to fall within the 95% confidence intervals. The slightly more restrictive SNR filter cutoff values of procedure 2 showed that the distribution of the data became skewed, which means that these values were also not normally distributed. This skew can probably be attributed to the loss of scaled $\overline{w'^2}$ values associated mainly with the low SNR signals and fewer high SNR signals. These largely extraneous signals were no doubt related to the ground clutter, electromagnetic interference, birds, and aircraft. The more restrictive SNR filter cutoff values of procedures 3 and 4 were affected by the loss of data, but in both cases the remaining data were found to be again normally distributed.

Conclusions

The proposed procedure as an extension of Angevine et al. (1994a) was able to eliminate poor quality measurements to produce reliable results. Key steps in this procedure were the imposition of suitable SNR filter cutoff values, the calculation of hourly floor values, and a reduction of this floor by removal of beam broadening and vertical shearing of horizontal wind effects.

In the course of determining $\overline{w'^2}$ values by the outlined procedure in this study, a similarity relationship was established by scaling $\overline{w'^2}$ and z by w_* and z_i , respectively. This relationship was shown to be similar in shape to but larger in magnitude than those of previous studies.

Acknowledgments

This research has been supported, in part, by the National Aeronautics and Space Administration (NAG8-1518) and by the National Science Foundation (ATM-9708622). This work was also supported by the U.S. Department of Energy, Office of Science, Office of Biological and Environmental Research, under contract W-31-109-Eng-38.

References

- André, J.-C., De Moor, G., Lacarrère, P., Thery, G., and du Vachat, R. (1978). "Modeling the 24-hour evolution of the mean and turbulent structures of the planetary boundary layer." *J. Atmos. Sci.*, 35, 1861–1883.
- Angevine, W. M., Avery, S. K., and Kok, G. L. (1993). "Virtual heat flux measurements from a boundary-layer profiler-RASS compared to aircraft measurements." *J. Appl. Meteorol.*, 32, 1901–1907.
- Angevine, W. M., Doviak, R. J., and Sorbjan, Z. (1994a). "Remote sensing of vertical velocity variance and surface heat flux in a convective boundary layer." *J. Appl. Meteorol.*, 33, 977–983.
- Angevine, W. M., White, A. B., and Avery, S. K. (1994b). "Boundary-layer depth and entrainment zone characterization with a boundary-layer profiler." *Boundary-Layer Meteorol.*, 68, 375–385.
- Coulter, R. L. (1979). "A comparison of three methods for measuring mixing-layer height." *J. Appl. Meteorol.*, 18, 1495–1499.
- Coulter, R. L., et al. (1999). "The Argonne Boundary Layer Experiments Facility: Using minisodars to complement a wind profiler network." *Meteorol. Atmos. Phys.*, 71, 53–59.
- Coulter, R. L., and Lesht, B. M. (1997). "Results of an automated comparison between winds and virtual temperatures from radiosonde and profilers." *Proc., 6th Atmospheric Radiation Measurement (ARM) Science Team Meeting*, U.S. Department of Energy, San Antonio, Tex., 59–60.

- Deardorff, J. W. (1974). "Three-dimensional numerical study of turbulence in an entraining mixed layer." *Boundary-Layer Meteorol.*, 7, 199–226.
- Doviak, R. J., and Zrnić, D. S. (1993). *Doppler radar and weather observations*, 2nd Ed., Academic, San Diego.
- Jacobs, J. M., Coulter, R. L., and Brutsaert, W. (2000). "Surface heat flux estimation with wind-profiler/RASS and radiosonde observations." *Adv. Water Resour.*, 23, 339–348.
- Lemone, M. A., et al. (2000). "Land-atmosphere interaction research, early results, and opportunities in the Walnut River watershed in southeast Kansas: CASES and ABLE." *Bull. Am. Meteorol. Soc.*, 81(4), 757–779.
- Lenschow, D. H., Wyngaard, J. C., and Pennell, W. T. (1980). "Mean-field and second-moment budgets in a baroclinic, convective boundary layer." *J. Atmos. Sci.*, 37, 1313–1326.
- Nastrom, G. D. (1997). "Doppler radar spectral width broadening due to beamwidth and wind shear." *Ann. Geophys.*, 15, 786–796.
- Smedman, A.-S., and Höögström, U. (1983). "Turbulent characteristics of a shallow convective internal boundary layer." *Boundary-Layer Meteorol.*, 25, 271–287.
- Stull, R. B. (1988). *An introduction to boundary layer meteorology*, Kluwer, Boston.
- Therry, G., and Lacarrère, P. (1983). "Improving the eddy kinetic energy model for planetary boundary layer description." *Boundary-Layer Meteorol.*, 25, 63–88.
- Wesely, M. L., Coulter, R. L., Klazura, G. E., Lesht, B. M., Sisterson, D. L., and Shannon, J. D. (1997). "A planetary boundary layer observational capability in Kansas." *Preprints 1st Symposium on Integrated Observing Systems*, American Meteorological Society, Boston, 138–140.